



HAL
open science

Improving constraints on the extended mass distribution in the Galactic Center with stellar orbits

Karim Abd El Dayem, Roberto Abuter, Nicolas Aimar, Pau Amaro Seoane, Antonio Amorim, Julie Beck, Jean Philippe Berger, Henri Bonnet, Guillaume Bourdarot, Wolfgang Brandner, et al.

► To cite this version:

Karim Abd El Dayem, Roberto Abuter, Nicolas Aimar, Pau Amaro Seoane, Antonio Amorim, et al.. Improving constraints on the extended mass distribution in the Galactic Center with stellar orbits. *Astron.Astrophys.*, 2024, 692, pp.A242. 10.1051/0004-6361/202452274 . hal-04725566

HAL Id: hal-04725566

<https://hal.science/hal-04725566v1>

Submitted on 16 Jan 2025



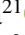
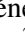
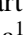
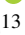


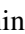




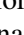



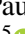




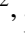
HAL is a multi-disciplinary open access archive for the deposit and dissemination of scientific research documents, whether they are published or not. The documents may come from teaching and research institutions in France or abroad, or from public or private research centers.

L'archive ouverte pluridisciplinaire **HAL**, est destinée au dépôt et à la diffusion de documents scientifiques de niveau recherche, publiés ou non, émanant des établissements d'enseignement et de recherche français ou étrangers, des laboratoires publics ou privés.



Distributed under a Creative Commons Attribution 4.0 International License

Improving constraints on the extended mass distribution in the Galactic center with stellar orbits

GRAVITY Collaboration^{*}: K. Abd El Dayem¹, R. Abuter⁴, N. Aimar^{1,7} , P. Amaro Seoane^{14,2,20,15}, A. Amorim^{8,7}, J. Beck², J. P. Berger^{3,4}, H. Bonnet⁴, G. Bourdarot², W. Brandner⁵, V. Cardoso^{7,17} , R. Capuzzo Dolcetta²¹ , Y. Clénet¹, R. Davies² , P. T. de Zeeuw , A. Drescher² , A. Eckart^{6,13} , F. Eisenhauer^{2,19}, H. Feuchtgruber², G. Finger², N. M. Förster Schreiber² , A. Foschi¹, F. Gao¹³, P. Garcia^{10,7} , E. Gendron¹, R. Genzel^{2,11}, S. Gillessen² , M. Hartl², X. Haubois⁹, F. Haussmann², G. Heißel^{16,1}, T. Henning⁵, S. Hippler⁵ , M. Horrobin⁶, L. Jochum⁹, L. Jocu³ , A. Kaufer⁹ , P. Kervella¹, S. Lacour^{1,4}, V. Lapeyrère¹, J.-B. Le Bouquin³, P. Léna¹ , D. Lutz², F. Mang², N. More², T. Ott², T. Paumard¹ , K. Perraut³ , G. Perrin¹, O. Pfuhl^{4,2}, S. Rabien², D. C. Ribeiro², M. Sadun Bordoni^{2,***} , S. Scheithauer⁵ , J. Shangquan² , T. Shimizu², J. Stadler^{12,2}, O. Straub^{2,18}, C. Straubmeier⁶ , E. Sturm², L. J. Tacconi², I. Urso¹ , F. Vincent¹, S. D. von Fellenberg^{13,2} , F. Widmann², E. Wieprecht², J. Woillez⁴, and F. Zhang^{22,23,24} 

(Affiliations can be found after the references)

Received 17 September 2024 / Accepted 12 November 2024

ABSTRACT

Studying the orbital motion of stars around Sagittarius A* in the Galactic center provides a unique opportunity to probe the gravitational potential near the supermassive black hole at the heart of our Galaxy. Interferometric data obtained with the GRAVITY instrument at the Very Large Telescope Interferometer (VLTI) since 2016 has allowed us to achieve unprecedented precision in tracking the orbits of these stars. GRAVITY data have been key to detecting the in-plane, prograde Schwarzschild precession of the orbit of the star S2 that is predicted by general relativity. By combining astrometric and spectroscopic data from multiple stars, including S2, S29, S38, and S55 – for which we have data around their time of pericenter passage with GRAVITY – we can now strengthen the significance of this detection to an approximately 10σ confidence level. The prograde precession of S2's orbit provides valuable insights into the potential presence of an extended mass distribution surrounding Sagittarius A*, which could consist of a dynamically relaxed stellar cusp comprising old stars and stellar remnants, along with a possible dark matter spike. Our analysis, based on two plausible density profiles – a power-law and a Plummer profile – constrains the enclosed mass within the orbit of S2 to be consistent with zero, establishing an upper limit of approximately $1200 M_{\odot}$ with a 1σ confidence level. This significantly improves our constraints on the mass distribution in the Galactic center. Our upper limit is very close to the expected value from numerical simulations for a stellar cusp in the Galactic center, leaving little room for a significant enhancement of dark matter density near Sagittarius A*.

Key words. black hole physics – gravitation – instrumentation: interferometers – Galaxy: center

1. Introduction

Since 2016, the GRAVITY interferometer at ESO's Very Large Telescope (GRAVITY Collaboration 2017) has allowed us to obtain astrometric data with unprecedented accuracy (reaching in the best cases a 1σ uncertainty of $30 \mu\text{as}$) of the S-stars orbiting around Sagittarius A* (Sgr A*) in the Galactic center (GC). This has turned them into a powerful tool to investigate the gravitational potential near the supermassive black hole (SMBH) at the center of our Galaxy, reaching distances from Sgr A* down to about a thousand times its Schwarzschild radius (R_S). Furthermore, astrometric and polarimetric observations of flares from Sgr A* with GRAVITY have revealed that the mass inside the flares' radius of a few R_S is consistent with the black hole mass measured from stellar orbits (GRAVITY Collaboration 2018b, 2023a). This, together with the radio-VLBI image of Sgr A*

(Event Horizon Telescope Collaboration 2022), confirms that Sgr A* is a SMBH beyond any reasonable doubt.

For the S2 star, due to its short orbital period of 16 years and its brightness ($m_K \approx 14$), astrometric data are available for two complete orbital revolutions around Sgr A*, while spectroscopic data cover one and a half revolutions (Schödel et al. 2002; Ghez et al. 2003, 2008; Gillessen et al. 2017). At the pericenter, S2 reaches a distance of $\sim 1400 R_S$ from the SMBH with a speed of $7700 \text{ km s}^{-1} \approx 0.026 c$. Monitoring the star's motion on the sky and radial velocity with GRAVITY and SINFONI around the time of the pericenter passage in 2018, crucial data were obtained in order to detect the first-order effects in the post-Newtonian (PN) expansion of general relativity (GR) on its orbital motion. The first one is the gravitational redshift of spectral lines, which was detected together with the transverse Doppler effect, predicted by special relativity, with a $\approx 10\sigma$ significance in GRAVITY Collaboration (2018a) and a $\approx 5\sigma$ significance in Do et al. (2019). GRAVITY Collaboration (2019) improved the significance of the detection to $\approx 20\sigma$. The other effect is the prograde, in-plane precession of the orbit's pericenter angle; namely, the Schwarzschild precession (SP). It

^{*} GRAVITY is developed in collaboration by MPE, LESIA of Paris Observatory/CNRS/Sorbonne Université/Univ. Paris Diderot, and IPAG of Université Grenoble Alpes/CNRS, MPIA, Univ. of Cologne, CENTRA – Centro de Astrofísica e Gravitação, and ESO.

^{**} Corresponding author; mbordoni@mpe.mpg.de

corresponds to an advance of $\delta\varphi_{Schw} = \frac{3\pi R_s}{a(1-e^2)}$ per orbit, which for S2 is equal to 12.1 arcmin per orbit in the prograde direction. In GRAVITY Collaboration (2020), this effect was detected at the 5σ level, and improved in GRAVITY Collaboration (2022) to $\approx 7\sigma$ by combining the data of S2 with data of the stars S29, S38, and S55, which could be observed with GRAVITY around the time of their pericenter passage and whose pericenter distances are comparable to that of S2.

The Lense-Thirring effect, caused by the spin of the central SMBH, appears at a 1.5PN order and gives both an additional contribution to the in-plane precession and a precession of the orbital plane (Merritt et al. 2010). We define $A_{LT} = 4\pi\chi \left(\frac{R_s}{2a(1-e^2)}\right)^{3/2}$, which for S2 is equal to 0.11 arcminutes. Consequently, the in-plane precession per orbit becomes $\delta\varphi_{Kerr} = \delta\varphi_{Schw} - 2A_{LT} \cos(i)$, while the precession per orbit of the orbital plane is given by $\delta\Phi_{Kerr} = A_{LT}$, where χ is the dimensionless spin of the SMBH (with $0 \leq \chi \leq 1$) and i is the angle between the direction of the SMBH spin and that of the stellar orbital angular momentum. The effect is thus at least 50 times smaller than the SP, assuming a SMBH with maximum spin, and is out of reach for current measurements. In order to measure the spin of Sgr A*, we would need to observe a star with a pericenter distance that is at least three times smaller than that of S2, given the astrometric accuracy achievable with GRAVITY (Waisberg et al. 2018; Capuzzo-Dolcetta & Sadun-Bordoni 2023).

Any extended mass distribution around Sgr A*, following a spherically symmetric density profile, would add a retrograde precession of the stellar orbits, counteracting the prograde SP (GRAVITY Collaboration 2020, 2022). This mass distribution is expected to be composed mainly of a dynamically relaxed cusp of old stars and stellar remnants. Peebles (1972); Frank & Rees (1976); Bahcall & Wolf (1976) first addressed the problem of the distribution of stars around a central massive BH. Bahcall & Wolf (1976) found that a single-mass stellar population around a central massive BH reaches a stationary density distribution over the two-body relaxation timescale, which is a power law, $\rho(r) \propto r^s$, with slope $s = -1.75$. In the GC, the old stellar population can be approximately represented by light stars with masses around $1 M_\odot$ and heavier stellar black holes with masses around $10 M_\odot$ (Alexander 2017). For such a population, mass segregation occurs, where heavier objects tend to concentrate toward the center due to dynamical interactions with lighter objects. The mass-segregation solution for the steady-state distribution of stars around a massive BH is derived in Alexander & Hopman (2009). It has two branches, weak and strong segregation, based on the dominance of heavier or lighter objects in the scattering interactions. In the weak segregation branch, the heavy objects settle into a power-law distribution with a slope of -1.75 , while the lighter objects exhibit a shallower profile with a slope of -1.5 , as was already heuristically derived in Bahcall & Wolf (1977). Conversely, the strong segregation branch results in steeper slopes and a larger difference between the light and heavy masses. The heavy masses settle into a much steeper cusp with $-2.75 \lesssim s \lesssim -2$, while the light masses settle into a cusp with $-1.75 \lesssim s \lesssim -1.5$. Preto & Amaro-Seoane (2010) provided a clear realization through N-body simulations of the strong mass segregation solution, showing also that the stellar cusp can develop on timescales that are much shorter than the relaxation time, which is shorter than the Hubble time for the GC (Alexander & Hopman 2009; Genzel et al. 2010). In Linial & Sari (2022), it is argued that weak segregation must exist interior to a certain break radius, r_B , where the massive population

dominates the scattering, while for radii larger than r_B the light objects dominate the scattering and strong segregation occurs.

The existence of such a stellar cusp in the GC is also validated by the observational results of Gallego-Cano et al. (2018) and Schödel et al. (2018) for the distribution of giant, subgiant, and main-sequence stars within the central few parsecs. They find that the density distribution of the light objects is shallower than $s = -1.5$, being compatible with a power-law with slope between -1.4 and -1.15 . This is impossible in the steady state, Bahcall & Wolf framework in order to maintain an equilibrium distribution, but could be explained by a number of factors, such as stellar collisions (Rose & MacLeod 2024), taking into account the complex star formation history of the nuclear star cluster (Baumgardt et al. 2018), or by diffusion in angular momentum leading to tidal disruptions; namely, diffusion into the loss cone (Zhang & Amaro-Seoane 2024). Red giant stars, instead, do not show a cusp but a distribution that appears to flatten toward the central ~ 0.3 pc (Buchholz et al. 2009; Do et al. 2009; Bartko et al. 2010; Gallego-Cano et al. 2018), possibly due to the stripping of red giant envelopes due to the interaction with a star-forming disk (Amaro-Seoane & Chen 2014).

In addition to the stellar cusp, an intermediate-mass black hole (IMBH) companion of Sgr A* could be present in the GC. It has been shown that an IMBH enclosed within the orbit of S2 can only have a mass of $< 10^3 M_\odot$ (GRAVITY Collaboration 2023b; Will et al. 2023). Moreover, it was predicted by Gondolo & Silk (1999) that dark matter particles could be accreted by the SMBH to form a dense spike, increasing the dark matter density in the GC by up to ten orders of magnitude with respect to the expected density in the case of a Navarro–Frenk–White (NFW) profile. In this scenario, the spike could contribute to the extended mass distribution around Sgr A*, while in the absence of such a spike, the contribution of dark matter within the radial range of the S-stars' orbits would be negligible under an NFW profile. The dark matter spike would also follow a power-law distribution, $\rho(r) \propto r^s$, with slope $-2.5 < s < -2.25$ in the case of a generalized NFW profile (Gondolo & Silk 1999; Shen et al. 2024). Another possibility that has been investigated is that dark matter could exist in the form of an ultralight scalar field or a massive vector field cloud that clusters around Sgr A* (Foschi et al. 2023; GRAVITY Collaboration 2024), or as a compact fermion ball supported by degeneracy pressure (Viollier et al. 1993; Argüelles et al. 2019; Becerra-Vergara et al. 2020).

Additionally, a deviation from general relativity, such as the one introduced by massive gravity theories or $f(R)$ -gravity, could modify the gravitational potential through a Yukawa-like correction in the Newtonian limit, adding an additional precession of the stellar orbits to the prograde SP and the retrograde precession induced by an extended mass distribution (Hees et al. 2017; De Martino et al. 2021; Tan & Lu 2024; Jovanović et al. 2024a,b). For the specific case of massive gravity, the additional precession would be prograde and equal to $\delta\varphi_\gamma = \pi\sqrt{1-e^2}\frac{a^2}{\lambda^2}$ (Jovanović et al. 2024a), where $\lambda = \frac{\hbar}{m_g c}$ is the Compton wavelength of the massive graviton, m_g the mass of the graviton, and \hbar the reduced Planck constant. From the observed precession of the S2 star, it is thus possible to derive a lower limit on λ and an upper limit on m_g , as is done in Hees et al. (2017); Jovanović et al. (2024a,b).

In GRAVITY Collaboration (2022), the 1σ upper limit on any extended mass distributed within the orbit of S2 is found to be $\approx 3000 M_\odot$, assuming a Plummer density profile (Plummer 1911). In this paper, we use S-star data, including one more year

of GRAVITY observations, in order to improve and extend the analysis conducted in GRAVITY Collaboration (2022). Our goal is to enhance the significance of the SP detection and to improve the observational constraints on the extended mass distribution around Sgr A*, comparing these results with theoretical models. In Section 2, we describe our dataset. We give our results for the SP detection in Section 3 and for the extended mass distribution in Section 4. In Section 5, we summarize our conclusions.

2. Observations

We describe in GRAVITY Collaboration (2022) how interferometric astrometry with GRAVITY confers many advantages over single-telescope AO imaging. Most importantly, it allows us to reach a much higher angular resolution and astrometric accuracy and to be significantly less affected by confusion noise. In this paper, we add one more year of GRAVITY data (up to September of 2022) for the stars S2, S29, S38, and S55 with respect to GRAVITY Collaboration (2022). In addition, since April 2023, the Enhanced Resolution Imager and Spectrograph (ERIS) has started to be operational at the VLT (Davies et al. 2023). This has made it possible, after the decommissioning of SINFONI (Eisenhauer et al. 2005) in 2019, to resume spectroscopic observations of the S-stars, with a new state-of-the-art AO system and a much higher spectral resolution ($R \sim 10\,000$, compared to $R \sim 4000$ of SINFONI). In this paper, we add to the long-standing SINFONI dataset the first radial velocity data points obtained with ERIS, during the commissioning phase in 2022.

For the analysis conducted in this paper, we used the following dataset:

- For S2, we used 128 NACO and 82 GRAVITY data points for the astrometry, and 92 SINFONI, 3 Keck, 2 NACO, 4 GNIRS/GEMINI, and 3 ERIS radial velocity measurements. These data cover the time span of 1992.2-2022.7.
- For S29, we used 66 NACO (2002.3-2019.7) and 29 GRAVITY data points (2019.6-2022.7) for the astrometry. We dropped a significant fraction of the available NACO data, which have been affected by confusion events. We also used 17 SINFONI and 2 GNIRS radial velocity measurements (2007.6-2021.4).
- For S38, we used 110 NACO (2004.2-2018.6) and 23 GRAVITY (2021.2-2022.7) data points for the astrometry, and 8 SINFONI, 2 Keck, and 1 ERIS data points for the radial velocity (2008.3-2022.4).
- For S55, we used 42 NACO (2004.5-2013.6) and 27 GRAVITY (2021.2-2022.6) astrometric data points, and 2 SINFONI radial velocity data points (2014).
- We also used the NACO and GRAVITY astrometric data and the SINFONI radial velocity data for other two stars: S24 and S42. For five other stars, S1, S4, S9, S21, and S13, we only used NACO and SINFONI data.

Figure 1 illustrates the orbits of all these stars. Details on the analysis of GRAVITY data can be found in Appendix A of GRAVITY Collaboration (2020). The analysis of spectroscopic data is described in Habibi et al. (2017) and GRAVITY Collaboration (2019).

3. Schwarzschild precession of the orbit of S2

3.1. Method

To test whether the orbits of S-stars are well described by a Schwarzschild orbit around Sgr A*, we modeled their

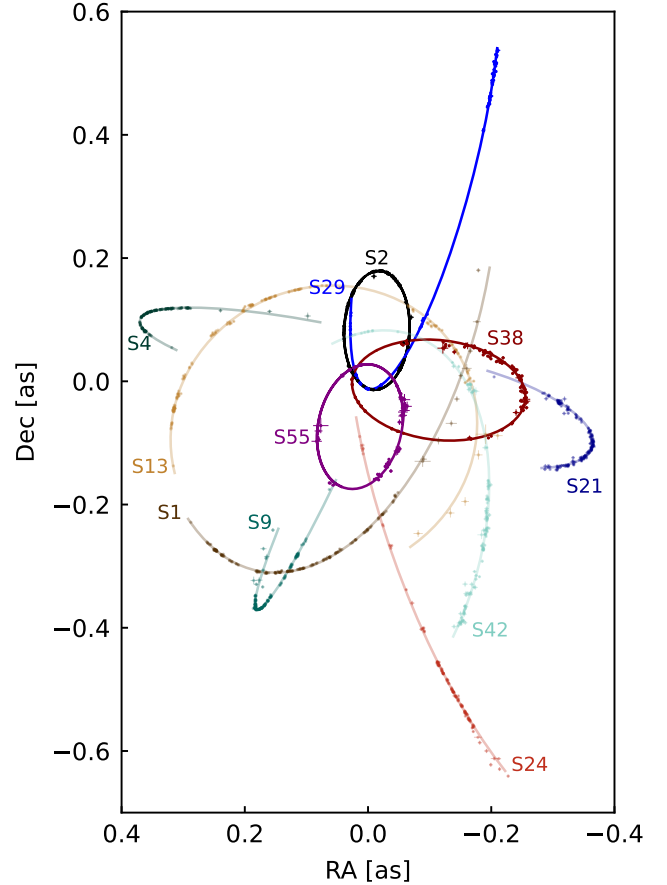


Fig. 1. Orbits for the set of 11 S-stars that have been used in this paper. Highlighted are the four most relevant stars to constrain the gravitational potential around Sgr A*: S2, S29, S38, and S55.

acceleration given by a first-order PN approximation of GR for a massless test particle (Will 1993) and multiplied the 1PN terms by a factor, f_{SP} , such that $f_{SP} = 0$ corresponds to a Keplerian closed (non-precessing) orbit and $f_{SP} = 1$ to a GR Schwarzschild orbit, with a prograde precession of the orbit's pericenter angle. The parameter, f_{SP} , was then used as a fitting parameter, together with the mass of and distance to the central SMBH, m_\bullet and R_0 , five coordinates $(x_0, y_0, vx_0, vy_0, vz_0)$ describing the position on the sky and three-dimensional velocity of Sgr A* in the AO imaging and spectroscopic reference frame, and six orbital parameters $(a, e, i, \omega, \Omega, t_0)$ for each star that we used in the orbital fit, describing the initial osculating Kepler orbit.

The orbital fitting was done using either a Levenberg-Marquardt χ^2 minimization algorithm or a (Metropolis-Hastings) Markov chain Monte Carlo (MCMC) analysis, using 200 000 realizations (for more details, see GRAVITY Collaboration 2018a, 2019, 2020).

3.2. Results

Here, we used the complete dataset of the stars S2, S29, S38, and S55 (Section 2) to obtain the best possible constraint on f_{SP} . As is noted in GRAVITY Collaboration (2020, 2022), the NACO zero points x_0, y_0, vx_0, vy_0 are partially degenerate with f_{SP} . To mitigate this degeneracy, we used data from seven additional S-stars (see Section 2 and Figure 1), performing a combined Keplerian fit to obtain an estimate for x_0, y_0, vx_0, vy_0 . We then combined the result for x_0, y_0, vx_0, vy_0 obtained from the stellar

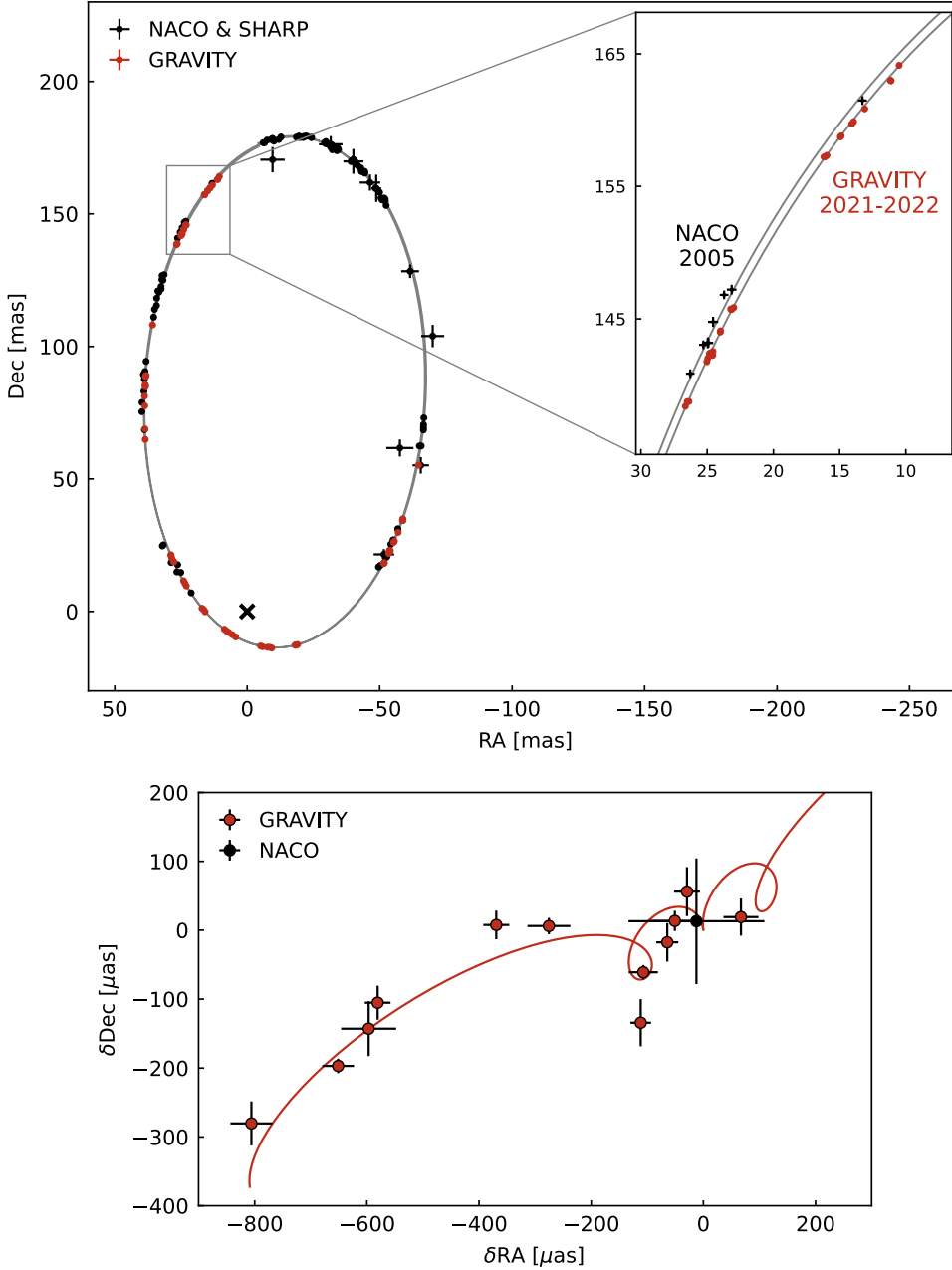


Fig. 2. The SP in the orbit of S2 around Sgr A*. Top: astrometric data of S2 obtained from 1992 to the end of 2022, together with the best-fitting orbit. The SHARP and NACO data are in black, while the GRAVITY data are in red. Sgr A* is located at (0,0), marked by a black cross. A zoom-in shows the effect of the prograde SP, comparing the GRAVITY 2021–2022 data with the NACO 2005 data. Bottom: residuals in RA and Dec between the best-fit Schwarzschild orbit ($f_{SP} = 1$) and the Newtonian component of the same orbit ($f_{SP} = 0$). In the plot, the Schwarzschild orbit predicted by GR corresponds to the loopy red curve. The corresponding residual GRAVITY data with respect to the Newtonian orbit are represented by red circles, and the NACO data by a black circle. The GRAVITY data points follow the Schwarzschild orbit predicted by GR. GRAVITY data are averages of several epochs. The NACO data have been averaged into one single data point.

orbits with the constraints from the NACO astrometry of flares and the prior from the construction of the AO reference frame (Plewa et al. 2015), in order to derive a prior for these parameters (see Appendix B).

Fitting the data of S2 using this prior for the NACO zero points, we obtain $f_{SP} = 0.918 \pm 0.128$ (MCMC $f_{SP} = 0.911 \pm 0.131$). The result improves when fitting the data of S2 together with S29, S38, and S55. In fact, these stars passed through the pericenter between 2021 and 2023, allowing us to observe them around the time of their pericenter passage with GRAVITY (GRAVITY Collaboration 2022). Their pericenter distances are comparable to that of S2, ranging from $1200 R_S$ to $2800 R_S$, providing crucial data to improve our constraints on the gravitational potential around Sgr A*. With this comprehensive dataset, we obtain $f_{SP} = 1.135 \pm 0.110$ (MCMC $f_{SP} = 1.133 \pm 0.113$). The significance of the SP detection has thus increased from $\approx 7\sigma$ of GRAVITY Collaboration (2022) to $\approx 10\sigma$. It is therefore strikingly evident that the orbit of S2 is, with ever stronger

significance, described by a Schwarzschild orbit around Sgr A*, exhibiting a prograde, in-plane precession of its pericenter angle. In the upper panel of Figure 2, we show the NACO and GRAVITY astrometric data of S2, highlighting the effect of the SP by comparing the GRAVITY 2021–2022 data with the NACO data from 2005, obtained one orbital period earlier. In the bottom panel, we show the averaged S2 residual data obtained with GRAVITY and NACO, after subtracting the Newtonian component of the best-fit Schwarzschild orbit. The data points follow the Schwarzschild orbit predicted by GR, which corresponds to the loopy red line in the plot.

For the first time, we have also been able to measure the SP of S2's orbit using only the GRAVITY astrometric data and the radial velocity data, due to the coverage of almost half of S2's orbit with GRAVITY. This allows us to completely exclude the NACO data from the fit and remove the NACO reference frame parameters x_0, y_0, vx_0, vy_0 , since with GRAVITY we can directly measure the separation vector between Sgr A* and S2.

Fitting the orbit of S2, we obtain $f_{SP} = 1.016 \pm 0.226$ (MCMC $f_{SP} = 1.024 \pm 0.260$), indicating a measurement of the SP with a $\approx 4\sigma$ confidence. This leads to a less significant detection than the one achieved by including the NACO data in the analysis, despite fitting four fewer parameters, which helps to reduce some degeneracies. In Appendix A, we attempt to predict how much we shall be able to improve our constraint on f_{SP} by continuing to monitor the orbit of S2 with GRAVITY and ERIS, carrying out mock observations. We show that GRAVITY data taken in the coming years, until the S2 star reaches the next apocenter passage in 2026, will only moderately improve the SP detection. Additionally, we show that the NACO imaging data will still be key in the near future in order to achieve the best possible constraint on f_{SP} , at least until S2 has gone through the next pericenter passage in 2034.

4. The extended mass distribution around Sgr A*

4.1. Method

To test the existence of an extended mass distribution around Sgr A*, we fixed $f_{SP} = 1$ (we assume a 1PN approximation of GR) and we modeled the extended mass distribution using a spherically symmetric density profile, $\rho(r)$. In this case, the motion of stars is not only due to the SMBH gravitational potential but also to the potential generated by this additional mass distribution, which gives an additional term to the stars acceleration and causes a retrograde precession of their orbits.

We chose to test two plausible density profiles:

- The power-law profile

$$\rho(r) = \rho_0 \left(\frac{r}{r_0} \right)^s, \quad (1)$$

where r_0 is a length scale for the radial coordinate (we fixed it to $r_0 = 40$ mpc), ρ_0 is the density at $r = r_0$, and s is the slope of the power law. Integrating, we obtain the enclosed mass as a function of the radius:

$$m(r) = \frac{4\pi\rho_0}{3+s} \left(\frac{r^{3+s}}{r_0^s} \right). \quad (2)$$

This is the distribution expected in the case of a stellar cusp, with a slope of $-2.75 \lesssim s \lesssim -1.5$ depending on the mass of the stellar population and whether weak or strong mass segregation occurs (Alexander & Hopman 2009; Preto & Amaro-Seoane 2010), and in the case of a dark matter spike, with a slope of $-2.5 < s < -2.25$ (Shen et al. 2024). We investigated this profile, varying the slope in the range $-3 < s \leq 0$. We thus explored a range of possible slopes for the density distribution, from a constant density profile, $\rho = \rho_0 = \text{const}$, for $s = 0$, to progressively steeper distributions with divergent central density for $s < 0$.

- The Plummer profile (Plummer 1911) is

$$\rho(r) = \rho_0 \left[1 + \left(\frac{r}{a} \right)^2 \right]^{-5/2}, \quad (3)$$

where a is the scale radius of the distribution, such that $\rho(r = a) = \frac{\rho_0}{2^{5/2}}$, and ρ_0 is the (finite) central density.

Integrating, we obtain the enclosed mass profile:

$$m(r) = \frac{4}{3} \pi \rho_0 a^3 \frac{(r/a)^3}{[1 + (r/a)^2]^{3/2}}. \quad (4)$$

The total mass of the distribution is equal to $m_{tot} = \frac{4}{3} \pi \rho_0 a^3$. We investigated this profile, varying the scale radius in the range $0 < a \leq 40$ mpc, going from very compact to progressively broader distributions, and thus also exploring the possibility that the density distribution reaches a plateau (a finite value $\rho(r = 0) = \rho_0$) at the center.

The procedure we adopted is the following. We parametrized both distributions by defining $\rho_0 = f_{pow} m_\bullet$ for the power law and $\rho_0 = \frac{f_{pl} m_\bullet}{\frac{4}{3} \pi a^3}$ for Plummer. In the first case, we fixed the slope, s , of the power law to different values in the interval $(-3, 0]$ and fit for the parameter f_{pow} , again together with m_\bullet , R_0 , the reference frame parameters, $x_0, y_0, vx_0, vy_0, vz_0$, and six orbital parameters ($a, e, i, \omega, \Omega, t_0$) per star. In the second case, we fixed the scale radius, a , of the Plummer profile to different values in the interval $(0, 40]$ mpc and fit for f_{pl} together with the other parameters. The orbital fitting was done using an MCMC analysis with 200 000 realizations. We did not allow the parameters s (for the power law) and a (for Plummer) to vary freely in the fit alongside f_{pow} and f_{pl} because doing so significantly increases the computational cost of the MCMC analysis, making it challenging to effectively explore the entire parameter space. It was assumed as a prior that $f_{pow} \geq 0$ and $f_{pl} \geq 0$, ensuring that the density is $\rho(r) \geq 0$ for every value of r . Then, we converted the resulting posterior distribution of the parameters f_{pow} and f_{pl} into a distribution on the parameter $M_{encl,S2} = m(r_{peri,S2} < r < r_{apo,S2})$; namely, the enclosed mass within the orbit of S2 (see Appendix B), where the pericenter distance of S2 is $r_{peri,S2} \sim 0.6$ mpc and the apocenter distance is $r_{apo,S2} \sim 9.4$ mpc. We focused on the enclosed mass within S2's orbit because it corresponds to the radial range over which the data used in the orbital fits lie. Presenting the results on the total mass of the Plummer distribution or the total mass of the power-law distribution within a radius of $r_{cut} \gg r_{apo,S2}$ is less relevant, as they depend on the chosen model for the density distribution and cannot be effectively constrained by our data. In addition, the mass enclosed within S2 pericenter $m(r_{peri,S2})$ is degenerate with the SMBH mass, m_\bullet , and for very steep distributions it is not well constrained with our data (see Appendix B).

4.2. Results

The fact that we observe a prograde, in-plane precession of S2's orbit, as is predicted by GR, implies that we can get strong constraints on the potential existence of an extended mass component distributed around Sgr A*. In fact, if such an extended mass component were present, it would induce a retrograde precession of S2's orbit, counteracting the prograde SP.

To test for the existence of an extended mass distribution around Sgr A*, we followed the procedure described in Section 4.1, performing a multi-star fit with the stars S2, S29, S38, and S55. For each star, we utilized the complete dataset available (Section 2), using both NACO and GRAVITY astrometric data. We imposed a prior on the NACO zero points x_0, y_0, vx_0, vy_0 , as in Section 3.2.

As was expected, we derived strong constraints on the enclosed mass within S2's orbit, $M_{encl,S2}$. The enclosed mass is compatible with zero, indicating that the orbits of the stars can be accurately described by Schwarzschild orbits without any extended mass surrounding the SMBH. In Figure 3, we plot the 1σ and 3σ upper limits (corresponding to 68.3% c.i. and 99.7% c.i., see Appendix B) on this parameter, as a function of the power-law slope (s) for a power-law distribution, and as a function of the Plummer scale radius (a) for a Plummer distribution.

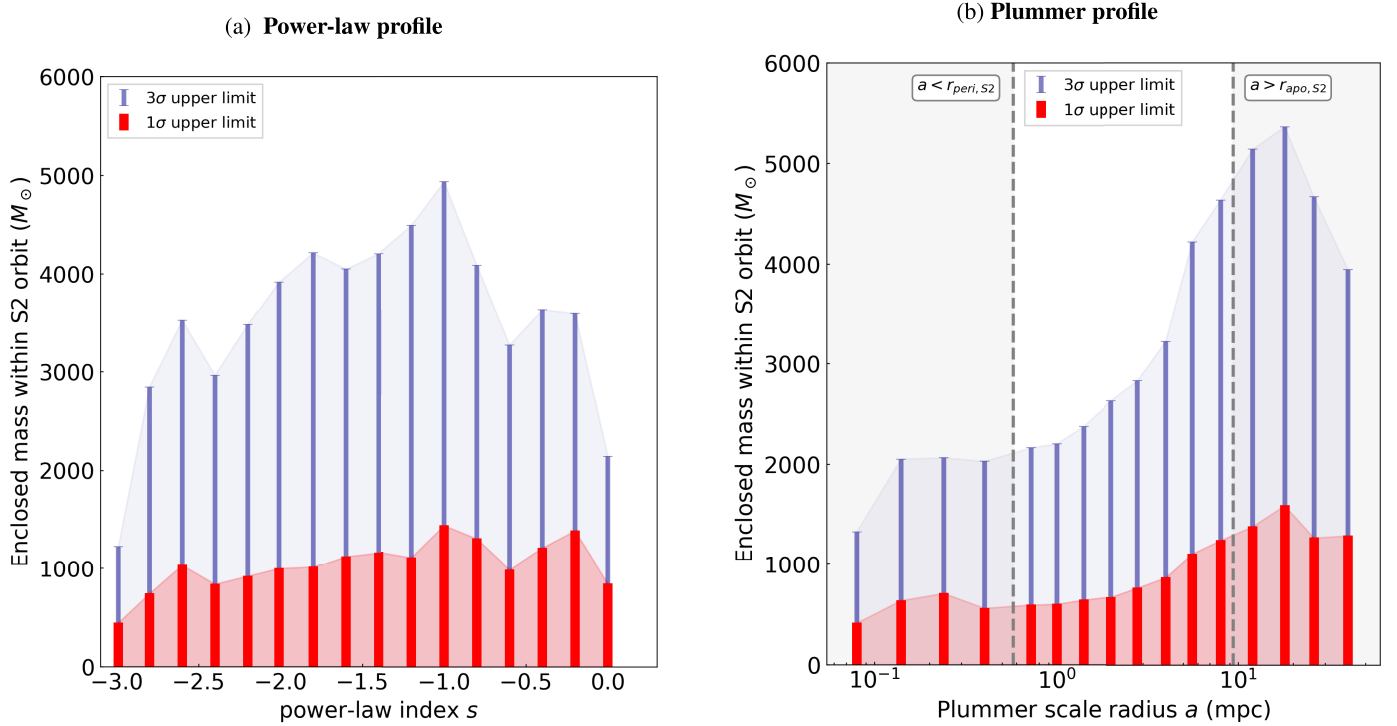


Fig. 3. Upper limit on the enclosed mass within the orbit of S2 for an extended mass distribution around Sgr A*. We tested two plausible density profiles for the mass distribution: a power-law profile with varying slope (panel a) and a Plummer profile with varying scale radius (panel b). In red, we plot the 1σ upper limit and in blue the 3σ upper limit, derived from a multi-star fit using data from the stars S2, S29, S38, and S55. Independently of the density profile, the enclosed mass within S2’s orbit is consistently compatible with zero. We set a strong upper limit of approximately $1200 M_{\odot}$ with a 1σ confidence level, for reasonable choices of the slope of the power law ($s < -1.2$) and the scale radius of the Plummer profile ($a \lesssim 8$ mpc).

We find that we cannot distinguish between different density profiles, as a power law with different slopes and a Plummer profile with different core radii fit the data equally well (we find no significant difference in χ^2). However, regardless of the specific density profile, we can reach a general conclusion. The 1σ upper limit on the enclosed mass within the orbit of S2 is lower than $\approx 1200 M_{\odot}$ for a power law with slope $s \lesssim -1.2$ and for a Plummer profile with scale radius $a \lesssim 8$ mpc, which corresponds approximately to the apocenter distance of S2. These constraints represent a significant improvement over the results found in [GRAVITY Collaboration \(2022\)](#), where the 1σ upper limit on any extended mass within S2’s apocenter was found to be $\approx 3000 M_{\odot}$. In addition, this can be translated into an upper limit on the amount of retrograde precession induced by the mass distribution, which we find to be $\lesssim 1$ arcmin per orbit and which is subdominant with respect to the prograde SP of ~ 12 arcmin per orbit. We emphasize that the data from S29, S38, and S55 are crucial for achieving such strong constraints (see [Appendix B](#) for a comparison with the results obtained from fitting the data of S2 only).

4.3. Comparison with theoretical models for the stellar cusp

We now compare our derived upper limit on the enclosed mass within the orbit of S2 to what is predicted for a dynamically relaxed stellar cusp in the GC. [Zhang & Amaro-Seoane \(2024\)](#) present a new Monte Carlo method that allows one to study the dynamical evolution of a star cluster with multiple mass components in the vicinity of a SMBH in a galactic nucleus. The code calculates the two-body relaxation process

based on two-dimensional (energy and angular momentum) Fokker-Planck equations and includes the effects of the loss cone, giving a more realistic result that what can be obtained in the steady-state framework of [Bahcall & Wolf \(1976, 1977\)](#); [Alexander & Hopman \(2009\)](#). Assuming a population of light objects with $m_l = 1 M_{\odot}$ and a population of heavy remnants with $m_h = 10 M_{\odot}$, they find consistent results with the mass segregation solution described in [Alexander & Hopman \(2009\)](#); [Preto & Amaro-Seoane \(2010\)](#). The heavy black holes sink toward the center due to dynamical friction and follow a steeper density profile, as is expected from mass segregation, reaching a slope between ~ -2.3 and ~ -1.7 in the inner regions. The light objects follow the expected slope of -1.5 if loss cone effects are ignored, while their density profile becomes shallower in the inner regions if the effects of the loss cone are included, reaching a slope of ~ -1.3 .

Here, we used an updated version of the code ([Zhang & Amaro-Seoane, in prep.](#)) that includes the potential from the stars and not only that of the central SMBH, in the calculation of the two-body relaxation of the energy and angular momentum of the particles in the simulation. This is particularly important for an accurate estimate of the density profile beyond the radius of influence of the SMBH, but also for the flux of particles into the loss cone. We considered a model with five components; namely, distinguishing between populations of stars of $m_s = 1 M_{\odot}$, brown dwarfs of $m_{bd} = 0.05 M_{\odot}$, white dwarfs of $m_{wd} = 0.6 M_{\odot}$, neutron stars of $m_{ns} = 1.4 M_{\odot}$, and stellar black holes of $m_{bh} = 10 M_{\odot}$, as in [Zhang & Amaro-Seoane \(2024\)](#). The fraction of brown dwarfs with respect to the stars at the beginning of the simulation is $f_{bd} = 0.2$, the fraction of white dwarfs is $f_{wd} = 0.1$, neutron stars $f_{ns} = 0.01$, and stellar black holes

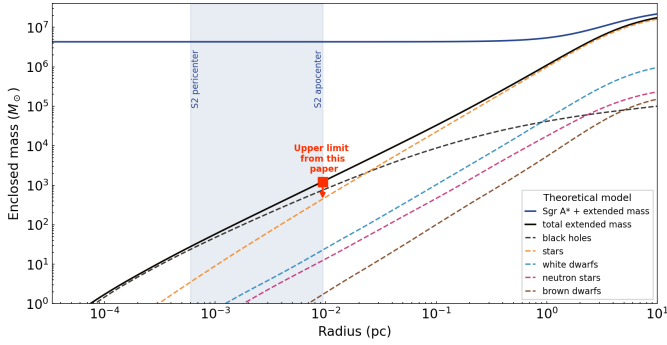


Fig. 4. Enclosed mass in the GC as a function of radius derived from numerical simulations, using an updated version of the code from Zhang & Amaro-Seoane (2024), for a model that includes stellar black holes, neutron stars, white dwarfs, brown dwarfs, and stars. The dashed colored lines show the predicted enclosed mass of each individual component, while the solid black line shows the total predicted enclosed mass considering all components. The predicted enclosed mass within S2’s orbit is in agreement with our 1σ upper limit of $\approx 1200 M_{\odot}$, indicated by the red square. The solid blue line shows the sum of the mass of Sgr A* to the total predicted enclosed mass. The shaded blue region illustrates the radial range of the orbit of S2.

$f_{bh} = 0.001$. The initial density profile in the simulation is a Dehnen model (Dehnen 1993) with $\gamma = 1$, total mass $M_{cl} = 3.2 \times 10^7 M_{\odot}$, and scale radius $r_a = 1.86$ pc. We let the system evolve for one relaxation time and find that the radius at which the total enclosed mass in the simulation equals $2m_{\bullet}$ — the radius of influence of the SMBH (Merritt 2013) — is $r = 3.9$ pc, consistent with findings from Chatzopoulos et al. (2014); Feldmeier-Krause et al. (2016). In Figure 4, we show the enclosed mass profile resulting from the simulations as a function of distance from the SMBH, comparing it with our observational results. The enclosed mass within the orbit of S2 predicted by the simulations is $m_{encl,S2} = 1210 M_{\odot}$, which is in agreement with our upper limit $m_{encl,S2} \lesssim 1200 M_{\odot}$ for a power-law density profile with slope $s < -1.2$. A similar result is obtained when considering a model with just two components; namely, stars of $1 M_{\odot}$ and stellar black holes of $10 M_{\odot}$, giving a total enclosed mass within S2’s orbit of $m_{encl,S2} = 1300 M_{\odot}$. Moreover, the simulations indicate that stellar mass black holes dominate the mass distribution in this region, contributing significantly to the total mass enclosed within the orbit of S2.

Since our upper limit is extremely close to the value predicted by simulations for a dynamically relaxed stellar cusp, we conclude that there is no substantial evidence for a significant enhancement of dark matter density near Sagittarius A*. However, it is important to note that, in principle, our orbital fits cannot distinguish between the mass contributions from the stellar cusp and a potential dark matter spike, as both are expected to follow similar power-law density distributions.

4.4. Note on the granularity of the stellar cusp

Our upper limit on the enclosed mass within S2’s orbit of $m_{encl,S2} \lesssim 1200 M_{\odot}$ is low enough to raise questions about whether modeling the extended mass distribution as a smooth, spherically symmetric density profile is a valid approximation. Figure 4 illustrates that, due to mass segregation, stellar black holes dominate the extended mass distribution within S2’s orbit. Therefore, we considered a scenario in which a finite number of bodies generate the extended potential by distributing the total

enclosed mass among N objects of equal mass. This configuration can lead to deviations in the orbital motion of S-stars compared to a smooth density distribution, as spherical symmetry is broken and scattering events may occur. In this case, there is not only in-plane precession but also precession of the orbital plane, as was discussed in Merritt et al. (2010).

An extreme case occurs when all the extended mass is concentrated in a single object, specifically an IMBH companion to Sgr A*. It has been shown that an IMBH within the orbit of S2 can only have a mass of $< 10^3 M_{\odot}$, in order to be compatible with observations (GRAVITY Collaboration 2023b; Will et al. 2023).

We assume that a cluster of 100 point-mass particles, each with a mass of $10 M_{\odot}$, is distributed within the apocenter of S2, following a power-law density distribution of the form $\rho(r) \propto r^{-2}$. We further assume that these particles are fixed in space and do not interact with one another. To assess the impact of this distribution on the orbit of S2, we conducted 100 mock observations of one full orbit of S2 around Sgr A* and the surrounding field objects, where each simulation corresponds to a different sampling of the field object positions to ensure adequate statistics. We then fit each simulated orbit for the f_{SP} parameter (see Section 3.1), obtaining a distribution with a mean and median of $f_{SP} = 0.94$, a standard deviation of 0.01, and a range of 0.09. When repeating this experiment with a cluster of 20 point-mass particles, each of $50 M_{\odot}$, we obtain a distribution with a mean and median of $f_{SP} = 0.95$, a standard deviation of 0.03, and a range of 0.23.

These results suggest that a distribution of stellar black holes around Sgr A* can in principle perturb our measurement of the SP, causing a deviation in S2’s orbit from the expected Schwarzschild orbit. This is an important effect to consider, especially as we achieve increasingly precise measurements of the SP using GRAVITY data, which have led to an error on f_{SP} of ~ 0.1 (Section 3.2). A detailed treatment of the effects of the granularity of the stellar cusp on stellar orbits is beyond the scope of this paper and will be addressed in detail in a forthcoming publication (Sadun Bordonni et al., in preparation).

5. Conclusions

In this paper, we have improved and extended the analysis conducted in GRAVITY Collaboration (2020, 2022), adding the new interferometric data obtained with GRAVITY in 2022. Particularly valuable, in addition to data for the well-known star S2, are data from the stars S29, S38, and S55. These stars have recently reached the pericenter of their orbits, allowing us to observe them around this critical phase with GRAVITY.

The orbital motions of S2, S29, S38, and S55 are perfectly compatible with Schwarzschild orbits around Sgr A* predicted by GR, exhibiting prograde, in-plane precession of their pericenter angles. By performing a multi-star fit with this data, we have detected the SP of their orbits with a confidence level of approximately $\approx 10\sigma$, marking a significant improvement over previous findings (GRAVITY Collaboration 2020, 2022).

We establish a stringent upper limit for the mass of any hypothetical extended mass distribution around Sgr A*, which would add a retrograde precession to the orbit of S2, counteracting the prograde, relativistic precession. This mass distribution could be composed of a dynamically relaxed cusp of old stars and stellar remnants and potentially of a dark matter spike. We modeled it with a spherically symmetric density distribution, testing two plausible density profiles; namely, a power law and a Plummer profile. We have found that, independently of the particular density profile, the enclosed mass within S2’s

orbit is consistently compatible with zero. We set a strong upper limit of approximately $1200 M_{\odot}$ with a 1σ confidence level, significantly improving upon the limits established in GRAVITY Collaboration (2022). Our findings align with theoretical predictions for a dynamically relaxed stellar cusp in the GC, composed of stars, brown dwarfs, white dwarfs, neutron stars, and stellar black holes, according to numerical simulations using an updated version of the code developed in Zhang & Amaro-Seoane (2024). This analysis predicts an enclosed mass of approximately $1210 M_{\odot}$ within S2's orbit. Given that our upper limit is very close to this predicted value, we conclude that we find no evidence for a significant dark matter spike in the GC.

S2 is currently moving toward the apocenter of its orbit, which it will reach in 2026. We expect that GRAVITY data collected in the coming years, combined with ERIS spectroscopy, will further refine our constraints on the extended mass distribution in the GC, as the mass distribution primarily influences stellar orbits in the apocenter half (Heiel et al. 2022). This will allow us to refine the comparison with the theoretical predictions for the stellar cusp, which is of fundamental importance in order to understand the distribution of the faint, old main-sequence stars and subgiants in the GC. These stars are too faint to be currently detected with GRAVITY, but their detection could be in reach of future observations with the GRAVITY+ upgrade at the VLTI (GRAVITY+ Collaboration 2022) and the MICADO instrument at the ELT (Davies et al. 2018). These stars could potentially be in tighter orbits around Sgr A* and could allow us to measure its spin and quadrupole moment. Furthermore, the comparison between our observational constraints and theoretical predictions is also important to better understand the distribution of compact objects in the GC and in galactic nuclei in general. This could offer precious insights in view of the future LISA mission (Amaro-Seoane et al. 2017), which will be able to detect the inspirals of compact objects into SMBHs (EMRIs) (Amaro-Seoane et al. 2007). In fact, the rate of EMRIs depends strongly on the density distribution of compact remnants within ~ 10 mpc of the central SMBH (Preto & Amaro-Seoane 2010), which corresponds to the apocenter distance of S2 for the GC.

Acknowledgements. We are very grateful to our funding agencies (MPG, ERC, CNRS [PNCG, PNGRAM], DFG, BMBF, Paris Observatory [CS, PhyFOG], Observatoire des Sciences de l'Univers de Grenoble, and the Fundao para a Cincia e Tecnologia), to ESO and the Paranal staff, and to the many scientific and technical staff members in our institutions, who helped to make NACO, SINFONI, and GRAVITY a reality. JS is supported by the Deutsche Forschungsgemeinschaft (DFG, German Research Foundation) under Germany's Excellence Strategy – EXC-2094 – 390783311. A.A., A.F., P.G. and V.C. were supported by Fundao para a Cincia e a Tecnologia, with grants reference SFRH/BSAB/142940/2018, UIDB/00099/2020 and PTDC/FIS-AST/7002/2020. F.W. has received funding from the European Union's Horizon 2020 research and innovation programme under grant agreement No 101004719. Based on observations collected at the European Southern Observatory under the ESO programme IDs 109.22ZA.005, 109.22ZA.002, 105.20B2.004, 0103.B-0032(C), 0101.B-0576(E), 0101.B-0576(C).

References

Alexander, T. 2017, *ARA&A*, 55, 17
 Alexander, T., & Hopman, C. 2009, *ApJ*, 697, 1861
 Amaro-Seoane, P., & Chen, X. 2014, *ApJ*, 781, L18
 Amaro-Seoane, P., Gair, J. R., Freitag, M., et al. 2007, *Class. Quant. Grav.*, 24, R113
 Amaro-Seoane, P., Audley, H., Babak, S., et al. 2017, *Laser Interferometer Space Antenna (ESA PUBLICATIONS DIVISION C/O ESTEC)*, submitted to ESA on January 13th in response to the call for missions for the L3 slot in the Cosmic Vision Programme
 Angilil, R., & Saha, P. 2014, *MNRAS*, 444, 3780

Arguelles, C. R., Krut, A., Rueda, J. A., & Ruffini, R. 2019, *Int. J. Mod. Phys. D*, 28, 1943003
 Bahcall, J. N., & Wolf, R. A. 1976, *ApJ*, 209, 214
 Bahcall, J. N., & Wolf, R. A. 1977, *ApJ*, 216, 883
 Bartko, H., Martins, F., Trippe, S., et al. 2010, *ApJ*, 708, 834
 Baumgardt, H., Amaro-Seoane, P., & Schdel, R. 2018, *A&A*, 609, A28
 Becerra-Vergara, E. A., Arguelles, C. R., Krut, A., Rueda, J. A., & Ruffini, R. 2020, *A&A*, 641, A34
 Buchholz, R. M., Schdel, R., & Eckart, A. 2009, *A&A*, 499, 483
 Capuzzo-Dolcetta, R., & Sadun-Bordoni, M. 2023, *MNRAS*, 522, 5828
 Chatzopoulos, S., Fritz, T. K., Gerhard, O., et al. 2014, *MNRAS*, 447, 948
 Davies, R., Alves, J., Clnet, Y., et al. 2018, *SPIE Conf. Ser.*, 10702, 107021S
 Davies, R., Absil, O., Agapito, G., et al. 2023, *A&A*, 674, A207
 Dehnen, W. 1993, *MNRAS*, 265, 250
 De Martino, I., della Monica, R., & De Laurentis, M. 2021, *Phys. Rev. D*, 104, L101502
 Do, T., Ghez, A. M., Morris, M. R., et al. 2009, *ApJ*, 703, 1323
 Do, T., Hees, A., Ghez, A., et al. 2019, *Science*, 365, 664
 Eisenhauer, F., Genzel, R., Alexander, T., et al. 2005, *ApJ*, 628, 246
 Event Horizon Telescope Collaboration 2022, *ApJ*, 930, L12
 Feldmeier-Krause, A., Zhu, L., Neumayer, N., et al. 2016, *MNRAS*, 466, 4040
 Foschi, A., Abuter, R., Aymar, N., et al. 2023, *MNRAS*, 524, 1075
 Frank, J., & Rees, M. J. 1976, *MNRAS*, 176, 633
 Gallego-Cano, E., Schdel, R., Dong, H., et al. 2018, *A&A*, 609, A26
 Genzel, R., Eisenhauer, F., & Gillessen, S. 2010, *Rev. Mod. Phys.*, 82, 3121
 Ghez, A. M., Duchne, G., Matthews, K., et al. 2003, *ApJ*, 586, L127
 Ghez, A. M., Salim, S., Weinberg, N. N., et al. 2008, *ApJ*, 689, 1044
 Gillessen, S., Plewa, P. M., Eisenhauer, F., et al. 2017, *ApJ*, 837, 30
 Gondolo, P., & Silk, J. 1999, *Phys. Rev. Lett.*, 83, 1719
 GRAVITY Collaboration (Abuter, R., et al.) 2017, *A&A*, 602, A94
 GRAVITY Collaboration (Abuter, R., et al.) 2018a, *A&A*, 615, L15
 GRAVITY Collaboration (Abuter, R., et al.) 2018b, *A&A*, 618, L10
 GRAVITY Collaboration (Abuter, R., et al.) 2019, *A&A*, 625, L10
 GRAVITY Collaboration (Abuter, R., et al.) 2020, *A&A*, 636, L5
 GRAVITY Collaboration (Abuter, R., et al.) 2022, *A&A*, 657, L12
 GRAVITY Collaboration (Abuter, R., et al.) 2023a, *A&A*, 677, L10
 GRAVITY Collaboration (Straub, O., et al.) 2023b, *A&A*, 672, A63
 GRAVITY Collaboration 2024, *MNRAS*, 530, 3740
 GRAVITY+ Collaboration (Abuter, R., et al.) 2022, *The Messenger*, 189, 17
 Habibi, M., Gillessen, S., Martins, F., et al. 2017, *ApJ*, 847, 120
 Hees, A., Do, T., Ghez, A. M., et al. 2017, *Phys. Rev. Lett.*, 118, 211101
 Heiel, G., Paumard, T., Perrin, G., & Vincent, F. 2022, *A&A*, 660, A13
 Jovanovi, P., Borka Jovanovi, V., Borka, D., & Zakharov, A. F. 2024a, *Symmetry*, 16, 397
 Jovanovi, P., Borka Jovanovi, V., Borka, D., & Zakharov, A. F. 2024b, *Phys. Rev. D*, 109, 064046
 Linial, I., & Sari, R. 2022, *ApJ*, 940, 101
 Merritt, D. 2013, *Dynamics and Evolution of Galactic Nuclei* (Princeton: Princeton University Press)
 Merritt, D., Alexander, T., Mikkola, S., & Will, C. M. 2010, *Phys. Rev. D*, 81, 062002
 Peebles, P. J. E. 1972, *ApJ*, 178, 371
 Plewa, P. M., Gillessen, S., Eisenhauer, F., et al. 2015, *MNRAS*, 453, 3234
 Plummer, H. C. 1911, *MNRAS*, 71, 460
 Preto, M., & Amaro-Seoane, P. 2010, *ApJ*, 708, L42
 Rose, S. C., & MacLeod, M. 2024, *ApJ*, 963, L17
 Schdel, R., Ott, T., Genzel, R., et al. 2002, *Nature*, 419, 694
 Schdel, R., Gallego-Cano, E., Dong, H., et al. 2018, *A&A*, 609, A27
 Shen, Z.-Q., Yuan, G.-W., Jiang, C.-Z., et al. 2024, *MNRAS*, 527, 3196
 Tan, Y., & Lu, Y. 2024, *Phys. Rev. D*, 109, 044047
 Viollier, R., Trautmann, D., & Tupper, G. 1993, *Phys. Lett. B*, 306, 79
 Waisberg, I., Dexter, J., Gillessen, S., et al. 2018, *MNRAS*, 476, 3600
 Will, C. M. 1993, *Theory and Experiment in Gravitational Physics* (Cambridge University Press)
 Will, C. M., Naoz, S., Hees, A., et al. 2023, *ApJ*, 959, 58
 Zhang, F., & Amaro-Seoane, P. 2024, *ApJ*, 961, 232

- ¹ LESIA, Observatoire de Paris, Universit PSL, CNRS, Sorbonne Universit, Universit de Paris, 5 place Jules Janssen, 92195 Meudon, France
- ² Max Planck Institute for Extraterrestrial Physics, Giessenbachstrae 1, 85748 Garching, Germany
- ³ Univ. Grenoble Alpes, CNRS, IPAG, 38000 Grenoble, France
- ⁴ European Southern Observatory, Karl-Schwarzschild-Strae 2, 85748 Garching, Germany

- ⁵ Max Planck Institute for Astronomy, Königstuhl 17, 69117 Heidelberg, Germany
- ⁶ 1st Institute of Physics, University of Cologne, Zùlpicher Straße 77, 50937 Cologne, Germany
- ⁷ CENTRA – Centro de Astrofísica e Gravitação, IST, Universidade de Lisboa, 1049-001 Lisboa, Portugal
- ⁸ Universidade de Lisboa – Faculdade de Ciências, Campo Grande, 1749-016 Lisboa, Portugal
- ⁹ European Southern Observatory, Casilla 19001, Santiago 19, Chile
- ¹⁰ Faculdade de Engenharia, Universidade do Porto, rua Dr. Roberto Frias, 4200-465 Porto, Portugal
- ¹¹ Departments of Physics & Astronomy, Le Conte Hall, University of California, Berkeley, CA 94720, USA
- ¹² Max Planck Institute for Astrophysics, Karl-Schwarzschild-Straße 1, 85748 Garching, Germany
- ¹³ Max Planck Institute for Radio Astronomy, auf dem Hügel 69, 53121 Bonn, Germany
- ¹⁴ Institute of Multidisciplinary Mathematics, Universitat Politècnica de València, València, Spain
- ¹⁵ Kavli Institute for Astronomy and Astrophysics, Beijing, China
- ¹⁶ Advanced Concepts Team, ESA, TEC-SF, ESTEC, Keplerlaan 1, 2201 AZ Noordwijk, The Netherlands
- ¹⁷ Niels Bohr International Academy, Niels Bohr Institute, Blegdamsvej 17, 2100 Copenhagen, Denmark
- ¹⁸ ORIGINS Excellence Cluster, Boltzmannstraße 2, 85748 Garching, Germany
- ¹⁹ Department of Physics, Technical University of Munich, 85748 Garching, Germany
- ²⁰ Higgs Centre for Theoretical Physics, Edinburgh, UK
- ²¹ Department of Physics, Sapienza, University of Rome, P.le A. Moro 5, 00185 Rome, Italy
- ²² School of Physics and Materials Science, Guangzhou University, Guangzhou 510006, PR China
- ²³ Key Laboratory for Astronomical Observation and Technology of Guangzhou, 510006 Guangzhou, PR China
- ²⁴ Astronomy Science and Technology Research Laboratory of Department of Education of Guangdong Province, Guangzhou 510006, PR China

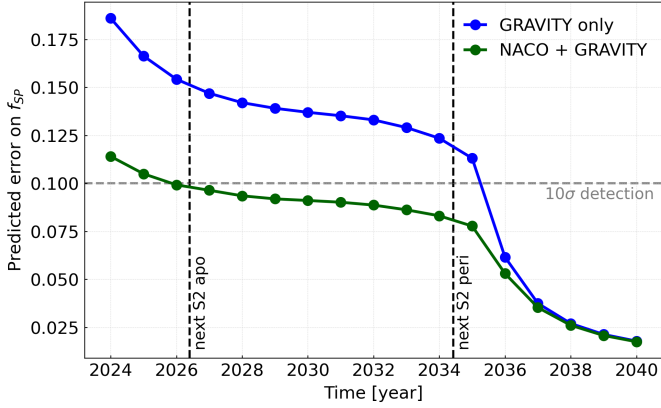


Fig. A.1: Predicted error on f_{SP} as a function of time, obtained through mock observations of S2 with GRAVITY and ERIS. The blue points show the result keeping only GRAVITY data in the fit, namely excluding the NACO data and removing the reference frame parameters. The green points show the result keeping both NACO and GRAVITY data.

Appendix A: Predicting the improvement on the SP detection with future observations

In order to predict how much we will be able to improve our constraint on the f_{SP} parameter by continuing to monitor the orbit of S2 with GRAVITY and ERIS, we carried out mock observations assuming that we will get, between March and September of each year (GC observing season from Paranal observatory):

- 10 GRAVITY data points per year with $50 \mu\text{as}$ astrometric accuracy,
- 3 radial velocity data points per year with ERIS with 10 km/s accuracy.

We then fit the actual S2 dataset together with the mock dataset and obtain a prediction on the error on f_{SP} in function of time. The result of this analysis is shown in Figure A.1. We compare the case in which we keep the NACO data in the fit with a prior on the reference frame parameters, with the case in which we use GRAVITY data only and we thus remove the reference frame parameters. This shows that GRAVITY data taken in the following years, until the S2 star will reach the next apocenter in 2026, will only moderately improve the SP detection. The predicted error remains then almost constant until ≈ 2034 , namely the time of the next pericenter passage of S2, and starts then to rapidly decrease. This is not surprising, because the SP happens mostly around pericenter (Angéilil & Saha 2014; GRAVITY Collaboration 2020; Heißel et al. 2022).

This analysis also tells us how valuable the NACO imaging data will still be in the near future, at least until S2 will reach the next pericenter passage in 2034. In fact, Figure A.1 shows that the constraint on f_{SP} will be stronger including NACO data in the orbital fit until a few years after the next pericenter passage of S2. In order to reach the same accuracy that we will be able to get on the SP detection keeping the NACO data in the fit, but using only GRAVITY data and eliminating the NACO zero points x_0, y_0, vx_0, vy_0 , we would need to wait until ≈ 2037 , when we will have observed two consecutive pericenter passages with GRAVITY.

Appendix B: Fit details

Table B.1: Best-fit parameters of the four-star fit determining f_{SP}

parameter	value	error	prior	error
M_\bullet [$10^6 M_\odot$]	4.2996	0.0118	-	-
R_0 [pc]	8275.9	8.6	-	-
x_0 [mas]	-0.72370	0.08707	-7.79×10^{-4}	7.38×10^{-5}
y_0 [mas]	-0.11921	0.07391	-1.18×10^{-4}	7.93×10^{-5}
vx_0 [mas/yr]	0.078241	0.005728	6.64×10^{-5}	7.27×10^{-6}
vy_0 [mas/yr]	0.040542	0.005620	3.70×10^{-5}	7.76×10^{-6}
vz_0 [km/s]	-1.9983	1.3325	0	5
f_{SP}	1.1350	0.1104	-	-

S2				
a [as]	0.12502	3×10^{-5}	-	-
e	0.88444	6×10^{-5}	-	-
i [°]	134.67	0.02	-	-
Ω [°]	228.21	0.03	-	-
ω [°]	66.279	0.029	-	-
t_{peri} [yr]	2018.3789	1×10^{-4}	-	-

S29				
a [as]	0.39025	9.4×10^{-4}	-	-
e	0.96880	9×10^{-5}	-	-
i [°]	144.24	0.09	-	-
Ω [°]	4.9259	0.1590	-	-
ω [°]	203.68	0.17	-	-
t_{peri} [yr]	2021.4102	$\times 10^{-4}$	-	-

S38				
a [as]	0.14249	4×10^{-5}	-	-
e	0.81807	2.2×10^{-4}	-	-
i [°]	168.69	0.19	-	-
Ω [°]	122.43	1.12	-	-
ω [°]	40.065	1.118	-	-
t_{peri} [yr]	2022.6843	8×10^{-4}	-	-

S55				
a [as]	0.10424	5×10^{-5}	-	-
e	0.72980	1.8×10^{-4}	-	-
i [°]	159.59	0.17	-	-
Ω [°]	319.43	0.97	-	-
ω [°]	327.77	0.93	-	-
t_{peri} [yr]	2009.4738	7.6×10^{-3}	-	-

Notes. The orbital elements are meant in the sense of osculating orbit parameters, using a conversion time close to the respective apocenter times, i.e., 2010.35 for S2, 1977 for S29, 2000 for S38, and 2012 for S55. The reference frame parameters x_0 and y_0 refer to the epoch 2000.

In Table B.1 we give the best-fit parameters of the four-star fit determining f_{SP} in Section 3.2.

In Figure B.1 we show an example of posterior distribution on the enclosed mass within S2's orbit, as derived from an MCMC analysis in the case of a multi-star fit with the stars S2, S29, S38 and S55. The 1σ upper limit on the enclosed mass corresponds to a 68.3 % confidence level, the 3σ upper limit to a 99.7 % confidence level.

In Figure B.2 we highlight that the mass enclosed within S2 pericenter is not well constrained with our data, as it is degenerate with the SMBH mass in the fitting. It depends severely on the steepness of the density profile.

In Figure B.3 we show the constraints on the enclosed mass

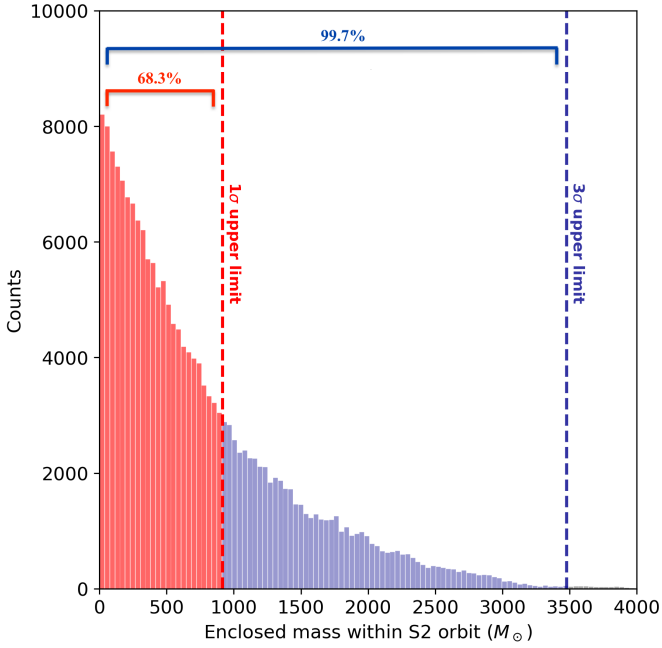


Fig. B.1: Example of posterior distribution on the enclosed mass within S2's orbit, for an MCMC analysis with 200 000 realizations, showing how the 1σ and 3σ upper limits are derived. This example corresponds to the case of a multi-star fit with the stars S2, S29, S38, S55 for a power-law density profile with slope $s = -2.2$.

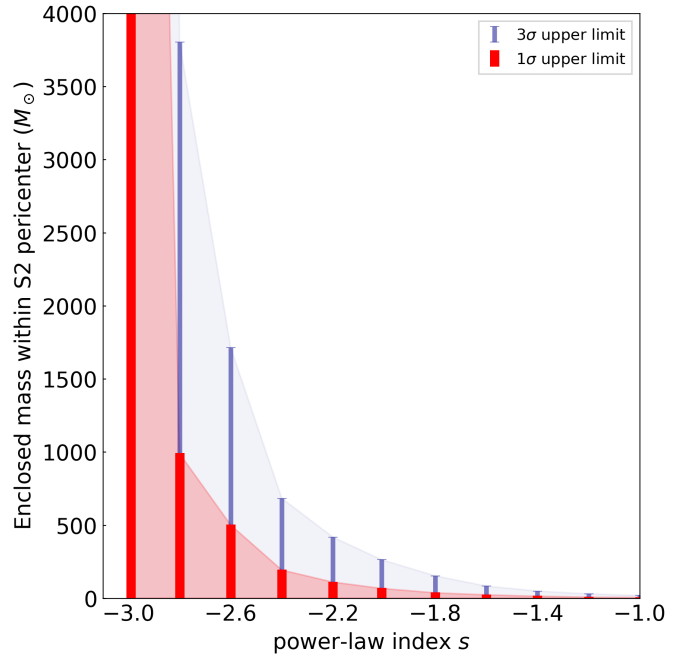


Fig. B.2: Enclosed mass within S2 pericenter for an extended mass distribution following a power-law density profile with varying slope. In red is plotted the 1σ upper limit and in blue the 3σ upper limit on this parameter, derived from a multi-star fit with the stars S2, S29, S38, S55.

within S2's orbit, obtained fitting the orbit of S2 only. Comparing Figure 3 with Figure B.3 it is immediately noticeable that a multi-star fit, namely fitting the data of S2 together with S29, S38 and S55, helps to obtain a much tighter constraint on the enclosed mass within S2's orbit than fitting the data of S2 only. The constraint is stronger for more compact distributions, namely for a steep power-law distribution and a Plummer profile with a small scale radius, and it becomes weaker for shallower distributions. This can be understood by translating the result on the enclosed mass into the amount of retrograde precession caused by this mass on the stellar orbits: the shallower the distribution, the larger is the amount of extended mass that can lie within the orbit of S2 inducing the same amount of retrograde precession.

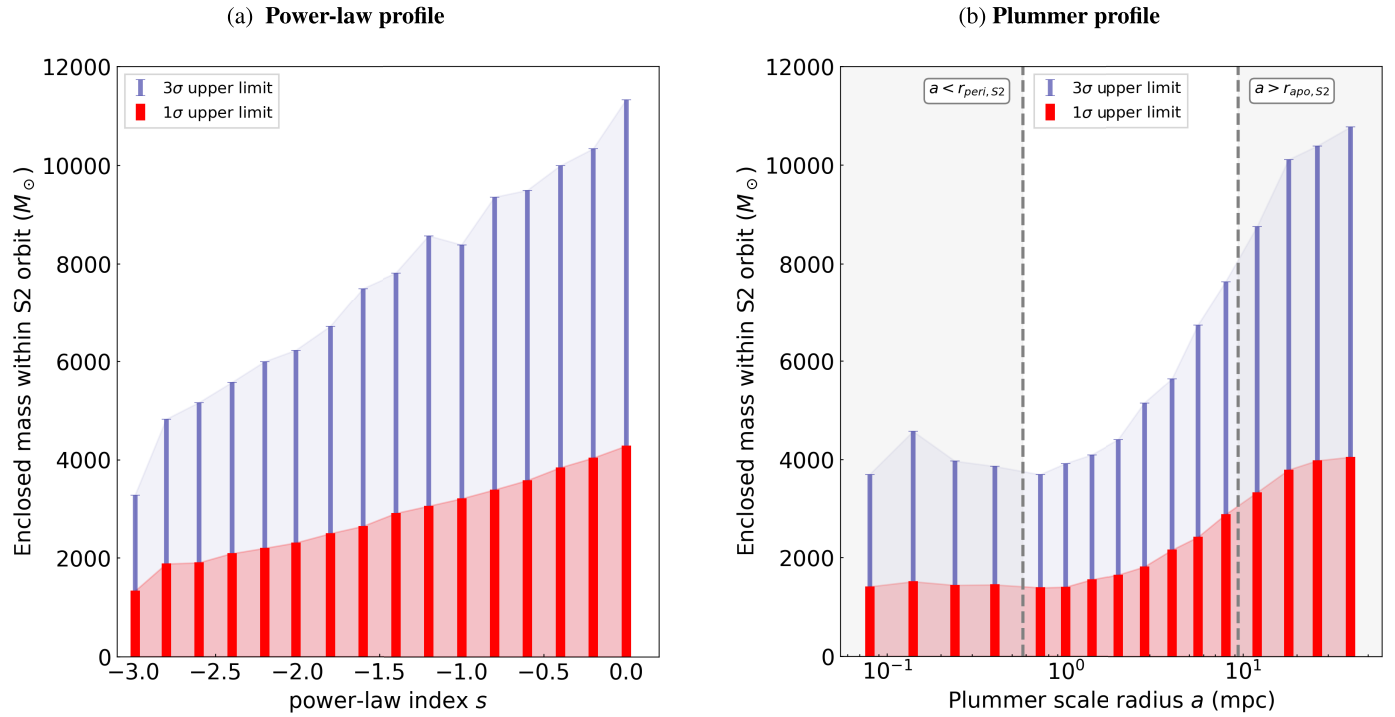


Fig. B.3: Enclosed mass within S2's orbit for an extended mass distribution following a power-law density profile with varying slope (a) and a Plummer density profile with varying scale radius (b). In red is plotted the 1σ upper limit and in blue the 3σ upper limit on this parameter, derived fitting the orbit of S2.